frontiers | Frontiers in Materials

TYPE Original Research
PUBLISHED 26 April 2024
DOI 10.3389/fmats.2024.1367251

OPEN ACCESS

EDITED BY
Haibo Li,
Ningxia University, China

REVIEWED BY
Lin Wei,
Lam Research, United States
Jingzhe Li,
Lam Research, United States

*CORRESPONDENCE
Xiaoxing Xiong,
xiaoxingxiong@whu.edu.cn
Liang Wei,
weiliang05@tkhealthcare.com

RECEIVED 08 January 2024
ACCEPTED 05 March 2024
PUBLISHED 26 April 2024

CITATION
Pu B, Deng L, Lu J, Wei L and Xiong X (2024), Anti-adhesion study of three-dimensional reconstructed carbon coatings.
Front. Mater. 11:1367251.
doi: 10.3389/fmats.2024.1367251

Anti-adhesion study of three-dimensional reconstructed carbon coatings

Bei Pu[1,2], Lusha Deng[3], Jun Lu[3], Liang Wei[2]* and Xiaoxing Xiong[1]*

[1]Department of Neurosurgery, Renmin Hospital of Wuhan University, Wuhan, China, [2]Transplantation Health Management Center, Sichuan Taikang Hospital, Chengdu, Sichuan, China, [3]Institute of Medical Materials Research, SKM Medical Instrument Co., Ltd., Chengdu, Sichuan, China

This research study focuses on the investigation of a three-dimensional reconstructed carbon coating based on stainless steel. The investigation encompasses the assessment of surface structure, elemental composition, cytotoxicity, and impact on wound healing. The findings indicate that the carbon coating possesses an approximate thickness of 700 nm, exhibiting a distinctive porous structure. Moreover, the surface water contact angle measures 97.7°, representing a 48.4° increase compared to uncoated stainless steel. Energy-dispersive spectroscopy (EDS) analysis confirms the uniform distribution of diverse elements on the coating's surface. Additionally, X-ray photoelectron spectroscopy (XPS) verifies a substantial carbon accumulation. The electrical resistance of the stainless steel remains largely intact after the application of the coating, as demonstrated by the four-probe method. Notably, *ex vivo* porcine liver tissue cutting experiments using carbon-coated electrosurgical pencil electrodes showed a significant anti-adhesion effect, with a reduction in tissue adhesions of 81.3%. Furthermore, the MTT test indicates no significant cytotoxicity associated with the carbon coating. Rat skin-cutting experiments further validate that the coating does not impede the process of wound healing. Overall, this study successfully validated the desirable properties of stainless steel-based 3D reconstructed carbon coatings, such as enhanced surface properties, improved anti-adhesion efficacy, negligible cytotoxicity, and compatibility with wound healing. These findings are important for advancing medical device technology and improving patient outcomes.

KEYWORDS

stainless steel, anti-adhesion, surface modification, electrosurgical electrode, carbon coating

1 Introduction

Stainless steels (SS) are extensively employed across diverse industries owing to their advantageous attributes, including ease of processing, cost-effectiveness, and resistance to corrosion, which hold substantial academic and industrial implications (Zuo et al., 2017; Akhtar et al., 2018). Within the medical domain, they are widely utilized in surgical instruments and medical implants, such as orthopedic and dental implants (Higuchi et al., 2006; Yan et al., 2020; Berbel et al., 2022). Nevertheless, the surface of stainless steel exhibits a propensity for cellular adherence and biofilm formation, resulting in contamination and suboptimal biocompatibility, thereby attracting considerable attention (Teo et al., 2021).

To address these issues, various surface modification techniques have been used on stainless steel surfaces, including laser surface modification (Balla et al., 2018), plasma treatment, and coating deposition (Sun et al., 2021). Recent advancements in coated stainless steel for medical devices include the incorporation of biocompatible coatings like chitosan/fluoride-doped diopside nanocomposite coatings (Karimi et al., 2018), hydroxyapatite (Zhang et al., 2016a), titanium nitride (Wang et al., 2011; Chukwuike et al., 2021), and graphene (Zhou et al., 2017) to improve the interaction between stainless steel and biological tissues, reducing the risk of adverse reactions. Additionally, antimicrobial coatings such as silver nanoparticles or antimicrobial copper have been applied to inhibit bacterial growth on the stainless steel surface, thereby reducing the risk of device-related infections (Eby et al., 2009; Wang et al., 2016; Zhang et al., 2019; Liu et al., 2021), or drug-eluting layers have been employed to enable localized drug administration at the implantation site, preventing infection or promoting healing. These technological advances have significant implications for both academia and industry, improving their performance and expanding their applications in the medical field.

Energy surgical instruments are indispensable tools in today's surgical procedures, and the electrodes in contact with human tissues are basically made of SS, such as electrosurgical pens, bipolar forceps, and radiofrequency scalpels which have the advantages of fast cutting speed, good hemostatic effect, easy operation and wide range of applications. Nevertheless, during the surgical process, the electrodes are prone to reach temperatures higher than 100°C, and the phenomenon of tissue carbonization and adhesion to the electrodes occurs, due to the action of the high-frequency electric field, the surface tissue adhesion will be more tightly packed, which is difficult to remove cleanly (Zhang et al., 2016b; Han et al., 2017; Zheng et al., 2018). These tissue adhesions reduce the smoothness of the cut and the precision of the operation and also increase the risk of tearing adjacent tissues, leading to unnecessary bleeding and tissue damage (Lv et al., 2022). So the surgeon has to pause the operation to clean the adherent tissues on the electrodes or replace the electrodes, which affects the surgeon's surgical smoothness, prolongs the operation time, and increases the risk of the operation (Xiao and Shubing, 2019; Zhou et al., 2020). Therefore, it is necessary to improve the anti-adhesion function of electrodes for energy surgical instruments.

To improve the performance of electrosurgical devices, some studies have explored various methods. These include the addition of auxiliary devices such as drip devices, coolant circuits, and ultrasonic vibration (Yao et al., 2021). Surface microstructure reshaping (Lin et al., 2017), has also been studied, particularly using bionic structures like sharkskin, lotus leaf, corn leaf, soursop leaf, and hogweed (Jiang et al., 2021). Surface coatings have been investigated for surface modification, including polytetrafluoroethylene (PTFE), chromium nitride (CrN) surface coating, and hydrogenated copper-containing diamond-like film (DLC-Cu) (Ou et al., 2014). Additionally, a combination of coating plus surface micro-modification and surface micro-structure plus lubricant (Lv et al., 2022). The use of these modified electrodes provides some protection against adhesion, ease of cleaning, and better durability than regular SS electrodes. This can increase surgical efficiency and improve the surgeon's surgical experience. For example, the addition of assistive devices, such as ultrasonic vibration, can reduce tissue adhesion by up to 80%, which achieves a good anti-adhesion effect. (Yao et al., 2018; Yao et al., 2021). In addition, some studies have attempted to achieve anti-adhesion by simulating various bionic structures on the electrode surface. For example, etching the surface of an electrosurgical scalpel into a "papillae" structure resembling a lotus leaf reduces the surgical temperature, reduces thermal damage, and reduces water droplet adhesion to the surface by 75% compared to a smooth flat surface (Koch et al., 2009); a biomimetic model of a "Smooth Liquid Infused Porous Surface (SLIPS)" was constructed based on the lips of the hogshead, and applied to the surface of an SS scalpel to almost completely prevent blood adhesion.

However, the existing modified surfaces may bring many other negative effects, such as unfavorable surgical safety, increasing excessive cost, and non-lasting anti-adhesive effects, thus limiting their clinical applications. For example, the increase in the number of auxiliary devices to increase the size of electrodes has caused inconvenience to the surgeon's operation. The use of saline drip cooling may affect the patient's physiological environment, and a non-electrolyte flushing solution may lead to hemolysis and hyponatremia, increasing the risk of surgery. The coolant needs to be replenished promptly due to high temperatures and other factors. The process of micromodification of the surface microstructure is complex and costly, and the structure is easily damaged with the extension of cutting time. When the structure is destroyed, the anti-adhesion property is also lost. Among these anti-adhesion methods, electrode surface coating is effective and does not adversely affect operation. The process is relatively simple, feasible, and suitable for mass production. It does not alter the original structure of the scalpel. However, the current widely used coatings are still unable to effectively solve the problem of tissue adhesion on the scalpel surface. For example, PTFE-coated electrodes have low cutting efficiency and poor durability against tissue adhesion (Tesler et al., 2015). With increasing cutting time, the PTFE insulating coating on the electrode surface was gradually damaged by arc ablation, and the anti-adhesion effect disappeared after about 20 s (Wan et al., 2018).

In order to solve the above problems, this paper applies a three-dimensional reconstructed (Seto et al., 2014) carbon coating technology to the most frequently used electrosurgical monopolar electrodes. Through physical and chemical tests as well as animal experiments, it is demonstrated that this carbon coating has excellent anti-adhesion properties and is biocompatible, which effectively reduces the adherence of the tissue crusts on the surface of the electrodes during the surgical process, thus reducing the number of cleanings and saving the surgical time. This ensures a smoother procedure and reduces surgical risks.

2 Materials and methods

2.1 Preparation of sample

Argon, hydrogen, methane: Manufacturer: Sichuan Guanli Gas Technology Co., Ltd., with a purity of 99.999%. The 200 specimens of 303 SS electrodes were from Chengdu Bomei Medical Supplies Co. Ltd. These samples are characterized by an iron content

of 69.86 wt%, chromium content of 17.6 wt%, nickel content of 8.9 wt%, carbon content of 0.15 wt%, and other element content of 1.48 wt%. They have dimensions of 70 mm × 2.5 mm × 0.5 mm and a roughness of 150.00 nm. Subsequently, these SS electrodes underwent a meticulous cleaning process involving anhydrous ethanol and deionized water. The electrodes were then affixed vertically onto specialized quartz racks before being introduced into the chemical vapor deposition (CVD) reaction chamber.

Within the CVD deposition reaction chamber, argon was introduced into the tube at a flow rate of 5,000 sccm to evacuate residual air, and after a duration of 10 min, the argon flow rate was adjusted to 1,000 sccm. Concurrently, the heating module was activated, elevating the temperature of the deposition chamber to 1,000°C at a rate of 20°C/min, maintained for 5 min. The subsequent coating preparation ensued through a meticulously controlled four-step process. Initially, hydrogen (500 sccm) and methane (600 sccm) were injected into the tube, and after a 3-min reaction period, the flow of hydrogen and methane ceased. The argon flow rate was then increased to 5,000 sccm and sustained for 2 min. In the second step, the argon flow rate was adjusted to 1,000 sccm, hydrogen at 800 sccm, and methane at 1,000 sccm were introduced. After a 5-min reaction period, the flow of hydrogen and methane ceased, and the argon flow rate returned to 5,000 sccm for a 2-min duration. Subsequently, the argon flow rate was adjusted to 1,000 sccm for the third step, during which hydrogen at 1,000 sccm and methane at 1,300 sccm were introduced. After a 2-min reaction period, the flow of hydrogen and methane was halted. In the final step, the heating of the furnace tube was discontinued, allowing the system to undergo natural cooling to room temperature. Subsequently, the argon supply was terminated, and the SS electrodes were extracted from the furnace. Notably, the electrode surfaces manifested a consistently uniform and smooth gray coating as a consequence of the deposition process.

2.2 Characterization

Coating morphology analysis: The morphology, roughness, and thickness of the coating were examined using Atomic Force Microscopy (AFM) (SPM-9700HT, Shimadzu Corporation) in intermittent mode. Scanning Electron Microscopy (SEM) (Scientific Apreo 2C, Thermo) with an aluminum target was used to characterize the surface morphology of the coating after cleaning with argon ion etching for 30 s.

Coating elemental composition: Energy-dispersive X-ray spectroscopy (EDS) (Ultim Max65, OXFORD) was utilized to analyze elements ranging from Be4 to Cf98, while X-ray photoelectron spectroscopy (XPS) (Scientific K-Alpha, Thermo, America) was employed.

Coating resistivity: The resistivity of the coating was measured using a digital four-point probe tester (ST2253, Jingle) at temperatures of 37°C and 100°C.

Coating contact angle: Static contact angle measurements of stainless steel and the coating were conducted using a droplet shape analyzer (DSA100, KRÜSS, Germany). The contact angle measurement range was 0°C–180°C, with a resolution of ±0.01°C.

2.3 Weight of isolated tissue cutting adhesion

The subjects were fresh pig livers within 2 hours of isolation. Ten randomly selected coated electrodes and ten uncoated electrodes were used. The electrodes were used in the electric cutting mode at 60W to cut the pig liver. The cutting process was controlled to have the same cutting time and length as much as possible. The weight difference between the electrodes before and after cutting was recorded. After cutting, the electrode surface was cleaned using medical gauze to remove any adhered weight. Each electrode was subjected to ten repeated cuts, with each cut lasting 60 s, and the average weight of the adhered material was calculated. All the experimental operations were performed by the same experimenter.

2.4 Biocompatibility testing

Cell cytotoxicity test was performed by Weike Inspection Group Co., Ltd.

Fifty-seven healthy 8-week-old adult male Sprague Dawley rats weighing between 300 and 350 g were provided with sufficient food and water. Among them, 54 rats were divided into three experimental groups (D3, D7, and D14), and the remaining three rats were used as blank control groups. The rats were purchased from Chengdu Dashuo Laboratory Animal Co. Ltd.

On the day of surgery, the rats in the D3 experimental group were randomly divided into two groups: the coated group (9 rats) and the uncoated group (9 rats). Both groups were anesthetized, and the dorsal hair of the rats was shaved using electric hair clippers to expose the surgical area of the skin. The skin was then wiped with iodophor for disinfection. Four incisions measuring 2.0 cm in length were made, with 1.5 cm in front of and behind the rats, and 1.0 cm on the left and right sides of the rats. These incisions were marked using a marker.

For both the coated group (n = 9) and the uncoated group (n = 9), the skin was incised using a coated scalpel in the high-frequency scalpel electrode mode at 35 W. The incisions were sterilized using an iodophor and photographed for documentation. All procedures were performed by the same investigator. The same surgical procedure was repeated for groups D7 and D14.

A digital camera was used to record changes in the incision on days 0, 3, 7, and 14, and the wound healing rate (Fan et al., 2014) was calculated from the photographic measurements of the wound area using ImageJ software.

$$\text{Wound healing rate}\,(\%) = \frac{(A_0 - A_t)}{A_0} \times 100\%, \tag{1}$$

A_0-A_t are the initial wound area and the wound area at the specified time "t", respectively. Wound area was measured from the photographs using ImageJ software, and the average time for wound closure was calculated for each group of rats. Masson staining and HE staining were sent to Chengdu Aochuang Zhongyou Biotechnology co., ltd.

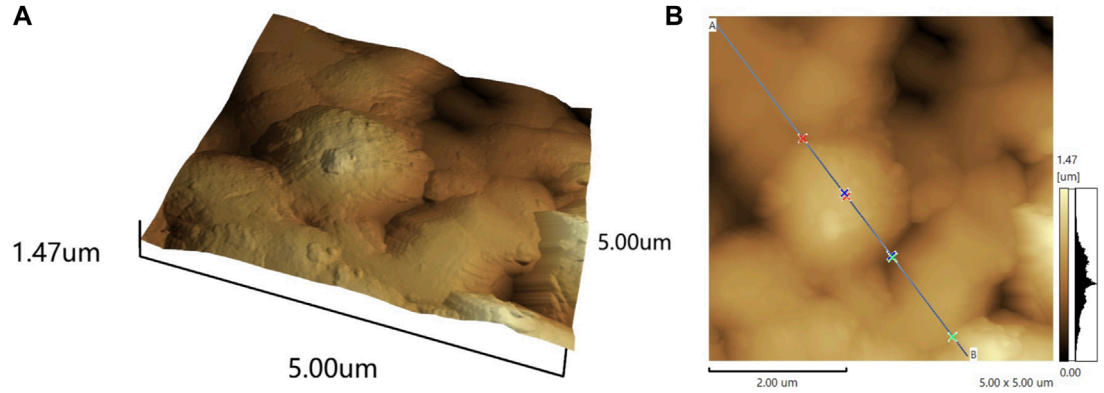

FIGURE 1
The 3D **(A)** and 2D **(B)** surface topography of the three-dimensional reconstructed carbon coating.

3 Results and discussion

3.1 Characterization

3.1.1 AFM

The AFM image reveals the topography of the film, as shown in Figure 1. Observation of the topography reveals that the coating exhibits non-uniformity at the microscale. It is noteworthy that within the measurement range, the maximum thickness of the coating is approximately 769.91 nm. Various parameters obtained from the AFM image allow for quantification of the surface's root mean square (RMS) roughness. Roughness signifies the smoothness mechanism of surface diffusion and is correlated with wetting properties, corrosion resistance, and other factors (Fauzi et al., 2020; Guo et al., 2021). The RMS roughness, calculated through cross-sectional profiles or surface analysis, measures 146.385 nm, which is similar to the roughness of the stainless steel utilized in the experiment, measured at 150.00 nm. This suggests that the presence of the coating does not significantly alter the surface roughness of the stainless steel.

3.1.2 SEM and contact angle

Figure 2 presented illustrates the comparative analysis of scanning electron microscope images portraying the surfaces of both coated and uncoated stainless steel. Upon observation, it becomes evident that the coated surface exhibits a rougher texture compared to the uncoated stainless steel. Furthermore, the coated surface showcases a considerable number of pores within its micro-nanostructure, which contributes to its distinctive three-dimensional architecture. The contact angle of the coated stainless steel was 97.7°, while the contact angle of the uncoated SS was 49.4°, and the coating significantly enhanced the hydrophobicity of the SS.

3.1.3 EDS

EDS analyses revealed a significant discrepancy in carbon content between the coated and 303 SS samples (Figure 3A). Specifically, the coating exhibited a markedly higher C content at 12.65%, compared to the mere 0.15% observed in the 303 SS. The detected elemental species, apart from C, remained consistent with the original composition of the SS. Notably, the Cr content in the coating registered at 31.78%, significantly surpassing the original 17.6% content in the stainless steel. Given chromium's established corrosion resistance, this discrepancy suggests that the coating has the potential to enhance the corrosion resistance of stainless steel (Yuan et al., 2017; Dong et al., 2019). Furthermore, the Fe concentration in the coating decreased to 50.33%, contrasting with the original SS value of approximately 70%, while the Ni concentration diminished from 8.9% to 2.39% (Figure 3B). This coating demonstrates the capability to deposit a carbon layer, concurrently altering the structure of the SS surface and modifying its elemental composition. This coating can deposit a carbon layer while changing the structure of the SS surface and changing its elemental composition. The reason for the structural change may be due to the thermal annealing of the stainless steel during the coating preparation process (Kim et al., 2014).

3.1.4 XPS

The analysis of the films' surfaces employing X-ray photoelectron spectroscopy (XPS) revealed disparities in elemental species and their quantities when compared to the results obtained from energy-dispersive X-ray spectroscopy (EDS) (Figure 4). These variations can be attributed to the different depths of detection, with EDS probing up to 1 μm and XPS providing data from a shallower depth of 5 nm. However, the XPS plots corroborate the substantial enrichment of carbon, further confirming the deposition of a significant amount of carbon in the coatings. Moreover, the presence of O1s peaks suggests that the films underwent oxidation upon exposure to the atmosphere. This oxidation phenomenon is indicated by the detection of oxygen species, signifying a chemical reaction between the film surface and atmospheric oxygen.

3.1.5 Electrical conductivity

Considering that the operating temperature of the electrodes can reach approximately 100°C, the resistance of both coated and uncoated SS samples was assessed using the four-probe method. The results, as presented in Table 1, demonstrate that the resistance and resistivity of the coated SS exhibit a slight increase compared to those of the uncoated SS, which may slightly affect the sharpness of the electrode during cutting.

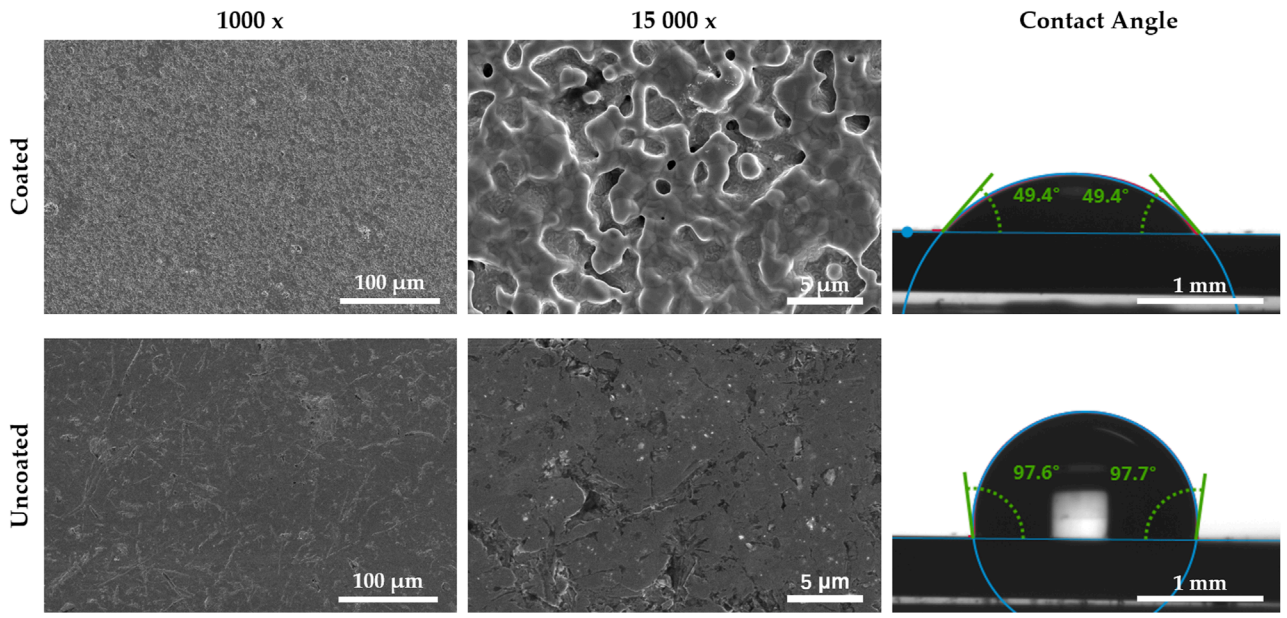

FIGURE 2
SEM morphologies and contact angles of coated stainless steel and uncoated stainless steel.

TABLE 1 A summary of the resistivity and resistance of uncoated and coated samples.

Temperature (°C)	Sample	Resistivity (uOhm ∗ m)	Resistance (mOhm)
37	Uncoated	0.795	3.869
	Coated	0.799	3.873
100	Uncoated	3.869	4.171
	Coated	3.873	4.201

3.2 Weight of isolated tissue cutting adhesion

As shown in Figure 5, after applying the coating, the weight of pig liver tissue adhering to the electrode during the cutting process was substantially reduced by 81.3%, which demonstrated the coating's excellent ability to prevent adhesion and promote tissue detachment. Compared to the uncoated electrodes, the coated electrodes had lower tissue adhesion and could be easily removed by gently wiping them with medical gauze. During 10 rounds of cutting for each electrode, the experimenters did not notice any morphological changes in the 3D reconstructed carbon coating, such as coating flaking and ablation, and the anti-adhesion properties remained virtually unchanged under prolonged use. It is expected that this result will reduce surgical interruptions and prolonged surgical time due to tissue adherence to the scalpel or the need for extensive wiping of crusts that can be applied to complex electrosurgical procedures. Thus, it offers the possibility of improving the surgeon's concentration and surgical efficiency, shortening the surgical time, and reducing the surgical risk.

In recent years, various coatings have been used to improve the anti-adhesive properties of SS surfaces, including polytetrafluoroethylene (PTFE), chromium nitride (CrN) surface coatings, and hydrogenated copper-containing diamond-like thin films (DLC-Cu) (Ou et al., 2016), but these coatings are usually unstable, easily damaged and harmful at high temperatures, unable to support prolonged surgeries and have a complicated and high-cost preparation process (Hsu et al., 2010). In contrast, the 3D reconstructed carbon coatings used in this study can be industrially produced at a controlled cost while significantly improving adhesion resistance, and the coatings are durable, easy to clean, and suitable for a variety of SS medical devices. However, to further evaluate the performance of 3D reconstructed carbon coatings in surgical electrodes, subsequent studies can use friction and wear testing machines to achieve real-time detection of cutting resistance at the surgical electrode-tissue interface during the process of electrode cutting to evaluate the cutting efficiency of the surgical electrodes. Meanwhile, SEM (Scanning Electron Microscope) images of the electrode cross-section morphology before and after cutting should be added, and measurements of the electrode temperature and tissue

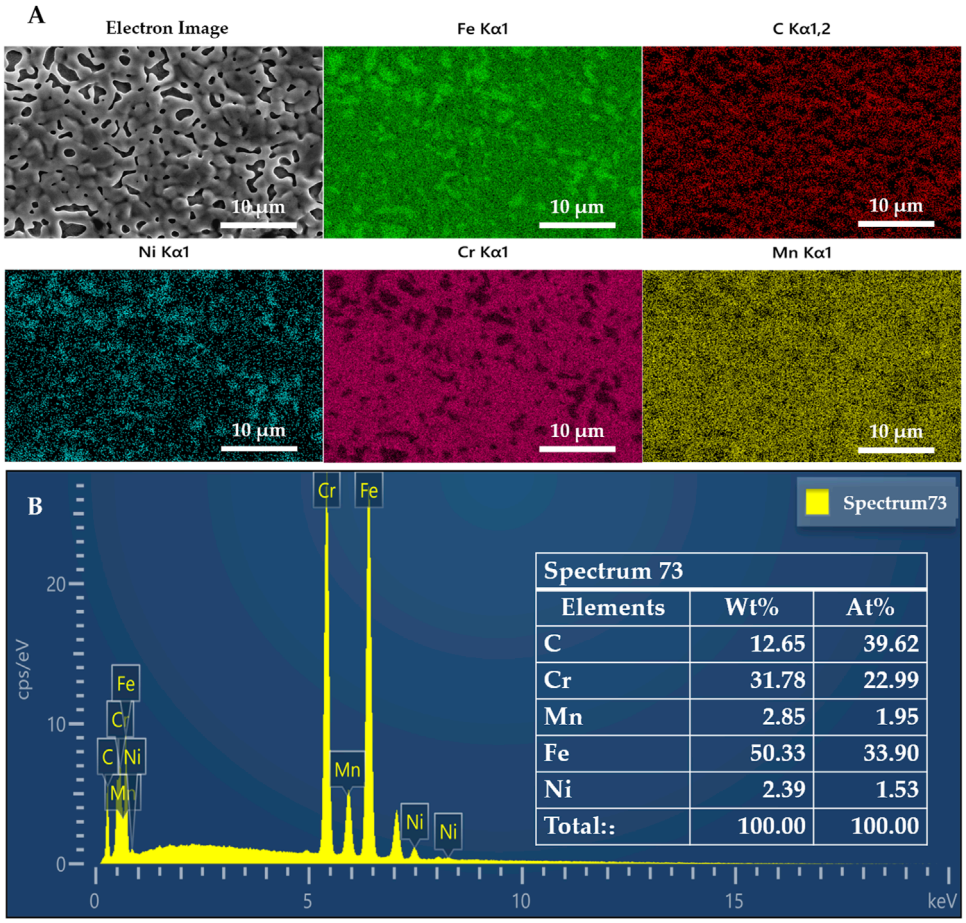

FIGURE 3
(A) EDS maps of metal elements confirming the uniform distribution of C (and all other elements) and **(B)** full spectra from the sample surface scaffold showing the presence of large amounts of C in the material.

thermal injury width after cutting should be conducted to perform corrosion resistance tests on the coatings.

3.3 Biocompatibility testing

Cytotoxicity tests showed that the relative cell viability of the coated sample extracts exceeded the criteria required by ISO standard 10993-5, indicating that it is free from potential cytotoxic effects, meets the *in vitro* cytotoxicity requirements for medical devices, and is expected to be used in stainless steel-based biomedical applications (Zhou et al., 2017).

Hemostasis, inflammation, proliferation, and remodeling are the four phases that occur sequentially throughout a wound healing process (Le et al., 2023) Immediately after tissue injury, the coagulation cascade is activated, and hemostasis is achieved by the formation of a clot of collagen, fibrin, and platelets, the fibrin clot acts as an initial scaffold for infiltrating cells, and the coagulation cascade continues with the release of many growth factors that activate the immune system. After achieving homeostasis and coagulation, wound healing enters the second phase of inflammation, where immune cells infiltrate the wound to clear pathogens and release cytokines that produce downstream signaling necessary for the recruitment of other cells and the production of extracellular matrix (EMC). The third phase of wound healing is characterized by new tissue formation and cellular proliferation, usually lasting between 2 and 10 days, where fibroblasts are recruited and begin to produce collagen and new blood vessels are formed following epithelial reformation. Remodeling is the final phase of wound healing and usually begins 2 weeks after injury, it involves scar contraction, ECM remodeling, and apoptosis, a process that can last for up to several years, so we focus on the Hemostasis, inflammatory, and proliferative phases of wound healing (Fan et al., 2014; Mandla et al., 2018; Rodrigues et al., 2019).

To evaluate the real wound-healing effect of 3D restructured carbon coating, a wound-healing assay *in vivo* was performed via a rat model. The following is a macroscopic and microscopic visualization analysis of wound healing after skin excision in rats using coated and uncoated high-frequency electrodes. The macroscopic images of wound healing on rats following day 0, day 3, day 7, and day 11 were captured and depicted as shown in Figure 6A, where the wound area of both coated and uncoated groups decreased with time and both wounds disappeared at day 11. Meanwhile, the wound healing rate (%) was calculated by measuring

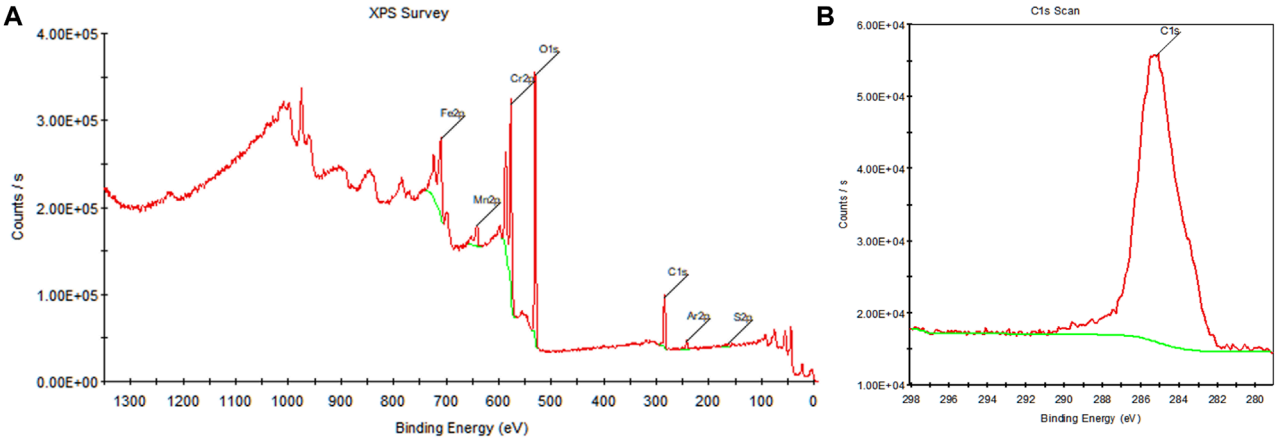

FIGURE 4
(A) Xps survey, **(B)** $C1_s$ scan.

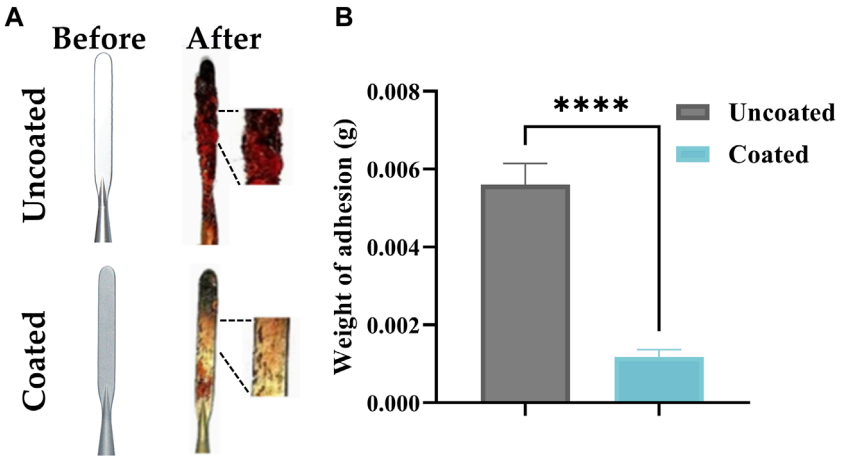

FIGURE 5
(A) Comparison of tissue adhesion between coated and uncoated electrodes, **(B)** Comparison of Weight of adhesion between coated and uncoated electrodes. The presented values are the experimental results on 10 electrodes for each group. Data are shown as the mean ± SEM, $****p \leq 0.0001$.

the area of skin defects at the determined time points, as shown in Figure 6B. During the healing process, the healing rates of the coated and uncoated groups were close to each other, both of which significantly accelerated after day 3, with a healing rate of more than 90% on day 7, and the wounds completely healed and disappeared on day 11. It should be noted that the wound healing rates of the coated group were 39.50% ± 3.89% and 92.83% ± 3.79% on the third and seventh days respectively, which were slightly higher than those of the uncoated group, which were 36.18% ± 3.13% and 90.53% ± 0.81% respectively. Therefore, the results suggest that the 3D reconstructed carbon coatings slightly enhanced the wound healing ability. Carbon coatings such as graphene and carbon nanotubes have been reported to have an antibacterial effect, and the same test can be performed on 3D reconfigured carbon coatings to verify whether they have the exact effect (Yaragalla et al., 2021; Shariati et al., 2023).

As shown in Figures 6C, D, fresh whole skin tissues on day 3, day 7, and day 14 were sectioned and stained with H&E and MT to assess the microscopic changes of wound recovery in the coated and uncoated groups. The H&E staining analysis in Figure 6C demonstrated that the skin surface structure was restored in both the coated and uncoated groups, and there was no significant difference in the pathological changes of epidermal thickening, inflammatory cell infiltration, fibrous tissue proliferation, neovascularization, and so on. There was no significant difference in epidermal thickening, inflammatory cell infiltration, fibrous tissue proliferation, neovascularization, and other pathological changes. In addition, the formation of collagen fibers was studied by MT staining, which showed that the amount of collagen deposited in the coated group was similar to that of the uncoated group, as indicated by the intense and evenly distributed blue staining (Figure 6D). As well known, collagen deposition was important during the wound

10.3389/fmats.2024.1367251

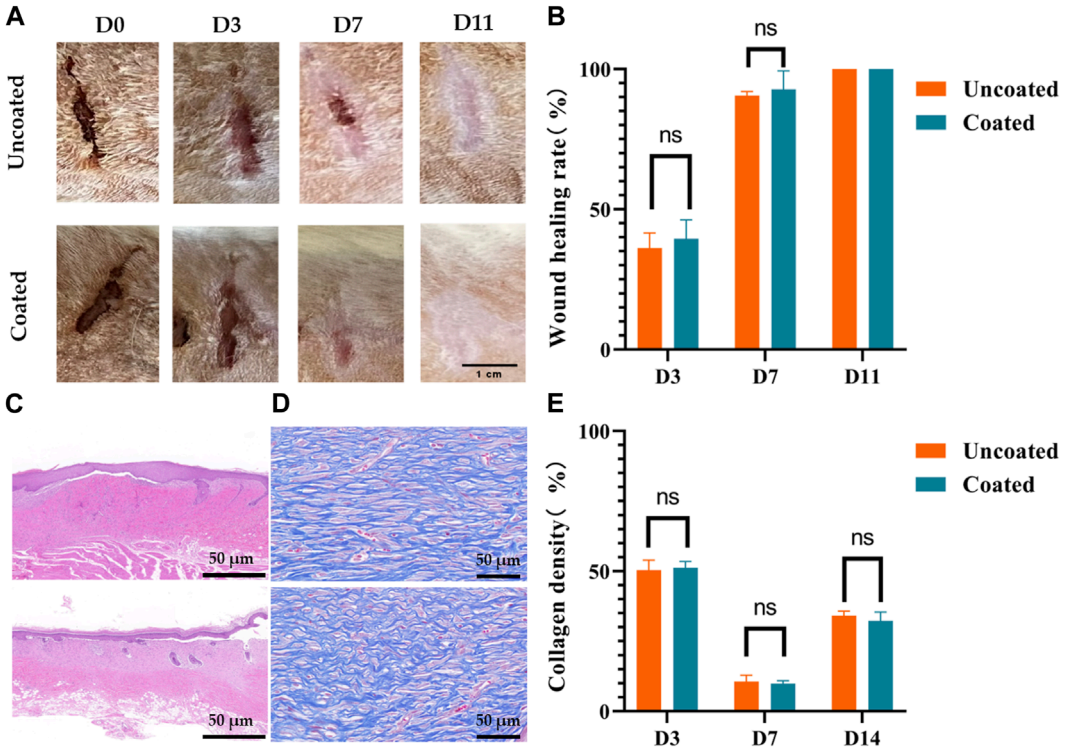

FIGURE 6
No affection for wound healing by coated electrodes in rats. **(A)** Progressive visualization of skin wound healing after cutting with coated and uncoated electrodes. **(B)** Changes in wound healing area, **(C)** Hematoxylin and eosin (H&E) staining of wound areas on day 14, scale bar 200μm, **(D)** Masson staining of wound areas on day 14, scale bar 20μm, **(E)** Quantitative result of collagen density of the coated *versus* uncoated group on day 14. The presented values are the experimental results on nine rats for each group. Data are shown as the mean ± SEM.

healing process (Sapru et al., 2021). Statistical quantitative analysis of collagen formation showed a similar course of blue density changes in the coated and uncoated groups (Figure 6E). There was no significant difference in collagen density between the uncoated and coated groups. These results suggest that our coated electrodes do not affect the wound-healing process.

4 Conclusion

This work reports a 3D reconstructed carbon coating based on SS. The coating increases the hydrophobicity of stainless steel and has a special surface structure without potential cytotoxicity. When applied to the electrode of an electrosurgical pencil, this coating demonstrates remarkable anti-adhesion and de-attachment properties. Consequently, it substantially diminishes the likelihood of surgical interruptions and prolonged procedure times caused by the adhesion of the electrosurgical pencil to tissue and the need for extensive scab wiping. This innovative solution offers a fresh avenue for enhancing the surgeon's focus and surgical efficiency, resulting in shorter operation durations and reduced surgical risks. Combined with the current research status and application needs of stainless steel in the field of medical devices, the follow-up research of this product can be carried out in the following aspects:

(1) The 3D reconfiguration of the carbon coating holds promise for exhibiting a certain level of bacteriostatic functionality. Subsequent investigations can involve the verification of this aspect through cell experiments and animal studies.
(2) In addition to addressing tissue adhesion, mitigating the issue of surgical smoke presents a significant challenge in energy-based surgeries. Further research can be undertaken to explore strategies aimed at minimizing the generation and dispersion of surgical smoke.
(3) Considering the wide range of applications of SS, the surface modification reported in this paper may also apply to other types of SS, which is expected to be used in biomedical fields such as surgical surgery, plastic surgery, dentistry, neurology, orthopedics, and so on.

Data availability statement

The raw data supporting the conclusion of this article will be made available by the authors, without undue reservation.

Ethics statement

All animal experimental protocols were approved by the Animal Experimentation Ethics Committee of Wuhan University and were conducted according to the Animal Care and Use Committee guidelines of Renmin Hospital of Wuhan University. The pig liver

samples used in this study were purchased from the local market, which is a conventional food industry product and therefore no specific ethical approval was required.

Author contributions

BP: Writing–review and editing, Writing–original draft. LD: Writing–original draft, Formal Analysis, Visualization. JL: Writing–original draft, Project administration. LW: Supervision, Writing–review and editing. XX: Supervision, Writing–review and editing.

Funding

The author(s) declare that no financial support was received for the research, authorship, and/or publication of this article.

Conflict of interest

Authors LD and JL were employed by SKM Medical Instrument Co., Ltd.

The remaining authors declare that the research was conducted in the absence of any commercial or financial relationships that could be construed as a potential conflict of interest.

Publisher's note

All claims expressed in this article are solely those of the authors and do not necessarily represent those of their affiliated organizations, or those of the publisher, the editors and the reviewers. Any product that may be evaluated in this article, or claim that may be made by its manufacturer, is not guaranteed or endorsed by the publisher.

References

Akhtar, S., Matin, A., Madhan Kumar, A., Ibrahim, A., and Laoui, T. (2018). Enhancement of anticorrosion property of 304 stainless steel using silane coatings. *Appl. Surf. Sci.* 440, 1286–1297. doi:10.1016/j.apsusc.2018.01.203

Balla, V. K., Dey, S., Muthuchamy, A. A., Janaki Ram, G. D., Das, M., and Bandyopadhyay, A. (2018). Laser surface modification of 316L stainless steel. *J. Biomed. Mater. Res. Part B Appl. Biomaterials* 106, 569–577. doi:10.1002/jbm.b.33872

Berbel, L. O., Viveiros, B. V. G. D., Micelli, A. L. P., Nigro, F., Rossi, J. L., and Costa, I. (2022). Corrosion mechanism of Ti-6Al-4V morse taper dental implants connected to 316 L stainless steel prosthetic abutment. *Mater. Today Commun.* 33, 104583. doi:10.1016/j.mtcomm.2022.104583

Chukwuike, V. I., Shtansky, D. V., and Subramanian, B. (2021). Biocompatibility study of nanocomposite titanium boron nitride (TiBN) thin films for orthopedic implant applications. *Surf. Coatings Technol.* 410, 126968. doi:10.1016/j.surfcoat.2021.126968

Dong, Z., Zhou, T., Liu, J., Zhang, X., Shen, B., Hu, W., et al. (2019). Cavitation erosion behaviors of surface chromizing layer on 316L stainless steel. *Ultrason. Sonochemistry* 58, 104668. doi:10.1016/j.ultsonch.2019.104668

Eby, D. M., Luckarift, H. R., and Johnson, G. R. (2009). Hybrid antimicrobial enzyme and silver nanoparticle coatings for medical instruments. *ACS Appl. Mater. Interfaces* 1, 1553–1560. doi:10.1021/am9002155

Fan, Z., Liu, B., Wang, J., Zhang, S., Lin, Q., Gong, P., et al. (2014). A novel wound dressing based on Ag/graphene polymer hydrogel: effectively kill bacteria and accelerate wound healing. *Adv. Funct. Mater.* 24, 3933–3943. doi:10.1002/adfm.201304202

Fauzi, N., Fen, Y. W., Saleviter, S., Mohd Daniyal, W., Hashim, H. S., Nasrullah, M., et al. (2020). Nanostructured chitosan/maghemite composites thin film for potential optical detection of mercury ion by surface plasmon resonance investigation. *Polymers* 12, 1497. doi:10.3390/polym12071497

Guo, L., Li, G., and Gan, Z. (2021). Effects of surface roughness on CMAS corrosion behavior for thermal barrier coating applications. *J. Adv. Ceram.* 10, 472–481. doi:10.1007/s40145-020-0449-7

Han, Z., Fu, J., Feng, X., Niu, S., Zhang, J., and Ren, L. (2017). Bionic anti-adhesive electrode coupled with maize leaf microstructures and TiO2 coating. *RSC Adv.* 7, 45287–45293. doi:10.1039/c7ra08184g

Higuchi, Y., Ohashi, Y., and Nakajima, H. (2006). Biocompatibility of Lotus-type stainless steel and titanium in alveolar bone. *Adv. Eng. Mater* 8, 907–912. doi:10.1002/adem.200600124

Hsu, Y. L., Lee, C. H., Chiu, S. M., Sung, Y. C., Yang, K. Y., and Chu, C. W. (2010). Anti-Sticking properties of PVD CrWNx, CrOx and ZrOx coatings on medical electrode application. *DDF* 297, 656–663. doi:10.4028/www.scientific.net/DDF.297-301.656

Jiang, C., Zhu, D., Wei, J., and Kong, L. (2021). Design of large-scale structural surfaces inspired by the peristome of nepenthes alata based on 3D printing. *J. Mech. Eng.* 57, 225. doi:10.3901/JME.2021.13.225

Karimi, S., Salahinejad, E., Sharifi, E., Nourian, A., and Tayebi, L. (2018). Bioperformance of chitosan/fluoride-doped diopside nanocomposite coatings deposited on medical stainless steel. *Carbohydr. Polym.* 202, 600–610. doi:10.1016/j.carbpol.2018.09.022

Kim, G.-T., Gim, S.-J., Cho, S.-M., Koratkar, N., and Oh, I.-K. (2014). Wetting-transparent graphene films for hydrophobic water-harvesting surfaces. *Adv. Mater.* 26, 5166–5172. doi:10.1002/adma.201401149

Koch, K., Bhushan, B., and Barthlott, W. (2009). Multifunctional surface structures of plants: an inspiration for biomimetics. *Prog. Mater. Sci.* 54, 137–178. doi:10.1016/j.pmatsci.2008.07.003

Le, L. T. T., Giang, N. N., Chien, P. N., Trinh, X.-T., Long, N.-V., Van Anh, L. T., et al. (2023). Enhancement of wound healing efficacy by chitosan-based hydrocolloid on Sprague Dawley rats. *Vivo* 37, 1052–1064. doi:10.21873/invivo.13180

Lin, C.-C., Lin, H.-J., Lin, Y.-H., Sugiatno, E., Ruslin, M., Su, C.-Y., et al. (2017). Micro/nanostructured surface modification using femtosecond laser pulses on minimally invasive electrosurgical devices. *J. Biomed. Mater. Res. Part B Appl. Biomaterials* 105, 865–873. doi:10.1002/jbm.b.33613

Liu, L. T., Li, Y. Z., Yu, K. P., Zhu, M. Y., Jiang, H., Yu, P., et al. (2021). A novel stainless steel with intensive silver nanoparticles showing superior antibacterial property. *Mater. Res. Lett.* 9, 270–277. doi:10.1080/21663831.2021.1894613

Lv, M., Song, L., Li, Y., Liu, J., Zhou, Y., Liu, J., et al. (2022). High quality anti-adhesion conductive electrotome. *Mater. Lett.* 313, 131750. doi:10.1016/j.matlet.2022.131750

Mandla, S., Davenport Huyer, L., and Radisic, M. (2018). Review: multimodal bioactive material approaches for wound healing. *Apl. Bioeng.* 2, 021503. doi:10.1063/1.5026773

Ou, K.-L., Chu, J.-S., Hosseinkhani, H., Chiou, J.-F., and Yu, C.-H. (2014). Biomedical nanostructured coating for minimally invasive surgery devices applications: characterization, cell cytotoxicity evaluation and an animal study in rat. *Surg. Endosc.* 28, 2174–2188. doi:10.1007/s00464-014-3450-9

Ou, K.-L., Weng, C.-C., Sugiatno, E., Ruslin, M., Lin, Y.-H., and Cheng, H.-Y. (2016). Effect of nanostructured thin film on minimally invasive surgery devices applications: characterization, cell cytotoxicity evaluation and an animal study in rat. *Surg. Endosc.* 30, 3035–3049. doi:10.1007/s00464-015-4596-9

Rodrigues, M., Kosaric, N., Bonham, C. A., and Gurtner, G. C. (2019). Wound healing: a cellular perspective. *Physiol. Rev.* 99, 665–706. doi:10.1152/physrev.00067.2017

Sapru, S., Das, S., Mandal, M., Ghosh, A. K., and Kundu, S. C. (2021). Sericin-chitosan-glycosaminoglycans hydrogels incorporated with growth factors for *in vitro* and *in vivo* skin repair. *Carbohydr. Polym.* 258, 117717. doi:10.1016/j.carbpol.2021.117717

Seto, T., Inoue, A., Higashi, H., Otani, Y., Kohno, M., and Hirasawa, M. (2014). Phase transition and restructuring of carbon nanoparticles induced by aerosol laser irradiation. *Carbon* 70, 224–232. doi:10.1016/j.carbon.2013.12.111

Shariati, A., Hosseini, S. M., Chegini, Z., Seifalian, A., and Arabestani, M. R. (2023). Graphene-based materials for inhibition of wound infection and accelerating wound healing. *Biomed. Pharmacother.* 158, 114184. doi:10.1016/j.biopha.2022.114184

Sun, L., Yuan, G., Gao, L., Yang, J., Chhowalla, M., Gharahcheshmeh, M. H., et al. (2021). Chemical vapour deposition. *Nat. Rev. Methods Prim.* 1, 5. doi:10.1038/s43586-020-00005-y

Teo, A. Q. A., Yan, L., Chaudhari, A., and O'Neill, G. K. (2021). Post-processing and surface characterization of additively manufactured stainless steel 316L lattice: implications for BioMedical use. *Materials* 14, 1376. doi:10.3390/ma14061376

Tesler, A. B., Kim, P., Kolle, S., Howell, C., Ahanotu, O., and Aizenberg, J. (2015). Extremely durable biofouling-resistant metallic surfaces based on electrodeposited nanoporous tungstite films on steel. *Nat. Commun.* 6, 8649. doi:10.1038/ncomms9649

Wan, J., Hao, R., Long, Y., and Zheng, L. (2018). Research on the variations of the incision efficiency and anti-sticking performance of PTFE-coated electrode with operation time. *JME* 54, 2. doi:10.3901/JME.2018.17.002

Wang, H., Tang, B., Li, X., and Ma, Y. (2011). Antibacterial properties and corrosion resistance of nitrogen-doped TiO2 coatings on stainless steel. *J. Mater. Sci. Technol.* 27, 309–316. doi:10.1016/S1005-0302(11)60067-4

Wang, Q., Ren, L., Li, X., Zhang, S., Sercombe, T. B., and Yang, K. (2016). Antimicrobial Cu-bearing stainless steel scaffolds. *Mater. Sci. Eng. C* 68, 519–522. doi:10.1016/j.msec.2016.06.038

Xiao, M., and Shubing, Hu (2019). Basic law of electrosurgical cutting and surface adhesion behavior of stainless steel electrode. *Zhongguo yi liao qi xie za zhi = Chin. J. Med. Instrum.* 43, 405–409. doi:10.3969/j.issn.1671-7104.2019.06.004

Yan, L., Lim, J. L., Lee, J. W., Tia, C. S. H., O'Neill, G. K., and Chong, D. Y. R. (2020). Finite element analysis of bone and implant stresses for customized 3D-printed orthopaedic implants in fracture fixation. *Med. Biol. Eng. Comput.* 58, 921–931. doi:10.1007/s11517-019-02104-9

Yao, G., Wu, W., Geng, D., and Zhang, X. (2021). Cutting performance of ultrasonic-assisted electrosurgical electrode. *J. Mech. Eng.* 57, 179. doi:10.3901/JME.2021.01.179

Yao, G., Zhang, D., Geng, D., and Jiang, X. (2018). Improving anti-adhesion performance of electrosurgical electrode assisted with ultrasonic vibration. *Ultrasonics* 84, 126–133. doi:10.1016/j.ultras.2017.10.015

Yaragalla, S., Bhavitha, K. B., and Athanassiou, A. (2021). A review on graphene based materials and their antimicrobial properties. *Coatings* 11, 1197. doi:10.3390/coatings11101197

Yuan, X., Zhao, Y., Li, X., and Chen, L. (2017). Effect of Cr on mechanical properties and corrosion behaviors of Fe-Mn-C-Al-Cr-N TWIP steels. *J. Mater. Sci. Technol.* 33, 1555–1560. doi:10.1016/j.jmst.2017.08.004

Zhang, P., Chen, H., Zhang, L., and Zhang, D. (2016b). Anti-adhesion effects of liquid-infused textured surfaces on high-temperature stainless steel for soft tissue. *Appl. Surf. Sci.* 385, 249–256. doi:10.1016/j.apsusc.2016.05.110

Zhang, S., Liang, X., Gadd, G. M., and Zhao, Q. (2019). Advanced titanium dioxide-polytetrafluorethylene (TiO2-PTFE) nanocomposite coatings on stainless steel surfaces with antibacterial and anti-corrosion properties. *Appl. Surf. Sci.* 490, 231–241. doi:10.1016/j.apsusc.2019.06.070

Zhang, X., Xiao, G., Liu, B., Jiang, C., Li, N., and Lu, Y. (2016a). The Formation of hydroxyapatite layer onto hopeite coating on stainless steel substrate. *Corros. Sci.* 111, 216–229. doi:10.1016/j.corsci.2016.05.012

Zheng, L., Wan, J., Long, Y., Fu, H., Zheng, J., and Zhou, Z. (2018). Effect of high-frequency electric field on the tissue sticking of minimally invasive electrosurgical devices. *R. Soc. Open Sci.* 5, 180125. doi:10.1098/rsos.180125

Zhou, C., Lu, J., and Wang, X. (2020). Adhesion behavior of textured electrosurgical electrode in an electric cutting process. *Coatings* 10, 596. doi:10.3390/coatings10060596

Zhou, H., Jiang, M., Xin, Y., Sun, G., Long, S., Bao, S., et al. (2017). Surface deposition of graphene layer for bioactivity improvement of biomedical 316 stainless steel. *Mater. Lett.* 192, 123–127. doi:10.1016/j.matlet.2016.12.043

Zuo, Y., Li, S., Zhao, X., and Tang, Y. (2017). Preparation and performance of a Pd-Co gradient coating on stainless steel. *Surf. Coatings Technol.* 330, 249–254. doi:10.1016/j.surfcoat.2017.09.064